Kinetic tracking of *Plasmodium falciparum* antigen presentation reveals determinants of protein export and membrane insertion

Short title: Malaria antigens RISE to the erythrocyte surface

Jinfeng Shao[1], Gunjan Arora[2], Javier Manzella-Lapeira[2], Joseph A. Brzostowski[2], and Sanjay A. Desai[1,*]

[1]Laboratory of Malaria and Vector Research and [2]Laboratory of Immunogenetics, National Institute of Allergy and Infectious Diseases, National Institutes of Health, Rockville, MD, USA

[*]Address correspondence to Sanjay A. Desai, sdesai@niaid.nih.gov

Abstract

Intracellular malaria parasites export many proteins into their host cell, inserting several into the erythrocyte plasma membrane to enable interactions with their external environment. While static techniques have identified some surface-exposed proteins, other candidates have eluded definitive localization and membrane topology determination. Moreover, both export kinetics and the mechanisms of membrane insertion remain largely unexplored. We introduce Reporter of Insertion and Surface Exposure (RISE), a method for continuous nondestructive tracking of antigen exposure on infected cells. RISE utilizes a small 11 aa NanoLuc fragment inserted into a target protein and detects surface exposure through high-affinity complementation. We tracked insertion of CLAG3, a malaria parasite protein linked to nutrient uptake, throughout the *P. falciparum* cycle in human erythrocytes. Our approach also revealed key determinants of trafficking and surface exposure. Removal of a C-terminal transmembrane domain aborted export. Unexpectedly, certain increases in the exposed reporter size improved surface exposure by up to 50-fold, revealing that both size and charge of the extracellular epitope influence membrane insertion. Insertion of parasite proteins at the host cell surface and antigen accessibility is regulated by multiple factors, enabling intracellular parasite survival and immune evasion under a broad range of conditions.

Introduction

Many viral, bacterial and parasitic microbes invade, grow, and replicate within host cells to evade immune detection, access host cell machinery for replication, and use cellular macromolecules as nutrient sources [1]. At the same time, the intracellular milieu limits the pathogen from accessing plasma nutrients and often provides an inhospitable ionic composition or acidic pH. To overcome these hurdles, intracellular pathogens often export effector proteins into their host cell to remodel their abode, altering host cell defenses and physiology to their benefit [2–4]. A subset of effector proteins then insert in the host membrane to enable pathogen interactions with the extracellular space. These exposed proteins serve diverse roles and are acknowledged vaccine and drug targets.

In the virulent human malaria parasite *Plasmodium falciparum*, surface-exposed proteins benefit pathogen replication by facilitating cytoadherence [5], immune evasion [6] and nutrient uptake [7]. These antigens have been identified through static assays such as confocal and electron microscopy techniques. Because these methods lack the required spatial resolution [8], they cannot unambiguously determine if some parasite proteins are surface-exposed or only adherent to the inner membrane face or cytoskeleton. In some cases, susceptibility to extracellular proteases or antibody-based assays with live cells can resolve this uncertainty [9,10], but these approaches also have limitations. Another approach, mass spectrometry-based identification after surface labeling with NHS esters [11], has yielded a largely unvalidated list of proteins that is complicated by increased NHS ester permeability after infection with *Plasmodium* spp. [12].

Currently available methods also suffer from an inability to track the timing and kinetics of antigen insertion at the host membrane, hindering molecular insights. Both surface exposure via

fusion of exocytic vesicles and "punch-through" insertion of soluble protein into the host membrane have been proposed [13,14], but the absence of direct and quantitative measurements has prevented definitive mechanistic insights.

To address these limitations and better define how pathogen proteins insert at their host cell membrane, we developed and used a Reporter of Insertion and Surface Exposure (RISE). Our study combines RISE with biochemical studies of the target reporter protein to identify constraints on protein trafficking and membrane insertion.

Results

HiBiT tagging within a conserved surface antigen in malaria parasites

We sought to generate a sensitive kinetic reporter for protein insertion on infected cells and chose human erythrocytes infected with the virulent *P. falciparum* malaria parasite. Indirect immunofluorescence microscopy assays (IFA) with antibodies against exposed epitopes offer a specific readout but suffer from low spatial resolution and provide limited kinetic information about protein export and host membrane insertion. Split enzyme reporters can overcome these limitations when one enzyme fragment is introduced into the exported protein; a specific signal is produced through complementation with a second fragment added extracellularly. Similar location-specific complementation has been described using mammalian proteins [15], but this approach has not been used to track appearance of pathogen-derived antigens on host cells. Because it relies on extracellular interactions with a surface-exposed epitope, our strategy resembles antigen presentation on immune effector cells [16].

The bright NanoLuc luciferase is an ideal enzymatic reporter for bloodstage *P. falciparum* studies [17] and has recently been optimized for development of a split reporter [18]. We

64 selected the 11 residue HiBiT and 18 kDa LgBiT fragments of NanoLuc for our studies, based
65 on their strong association (K_D = 700 pM) that yields an ATP-independent, furimazine-sensitive
66 luminescence signal.

67 We next reasoned that minimal modification of a normally exported parasite protein would
68 be more informative about parasite biology than extensively engineered reporters, as used
69 previously [19]. We preferred the parasite CLAG3 protein for these studies over antigens such as
70 PfEMP1 and RIFINs encoded by large multigene families to avoid epigenetic regulation and
71 variable expression [20]. *Clag* paralogs also undergo epigenetic silencing [21], but some clones
72 carry a single constitutively expressed hybrid *clag3* gene termed *clag3h* [22]. One such line,
73 KC5, has been successfully used for transfections without the risk of epigenetic silencing [23].
74 CLAG3 is also the only known surface-exposed protein conserved in all examined *Plasmodium*
75 spp. [24], suggesting that trafficking insights made using this protein may be broadly applicable.
76 Because CLAG3 expression is linked to the plasmodial surface anion channel (PSAC), an ion
77 and nutrient uptake channel at the host membrane [9], transport studies with transfectant parasites
78 would also provide a biochemical correlate of reporter signal activity. We therefore selected
79 CLAG3 for tagging and the KC5 clone for production of a surface exposure reporter parasite.

80 CLAG3 has a small 10-30 aa hypervariable region that appears to be exposed at the host
81 membrane (HVR, Fig 1A) [25]. We therefore used CRISPR/Cas9 editing to replace the KC5
82 *clag3h* HVR sequence with a single HiBiT tag flanked by 8 aa linker sequences; we named this
83 limiting dilution clone *8-1* based on the size of the flanking linker and the number of inserted
84 HiBiT tags (Fig 1A, bottom). HVR replacement increased the size of the extracellular loop
85 domain by a modest 10 residues (S1A Fig). We also produced *8-1HA*, a similar line with an HA
86 epitope tag added after the HiBiT linker cassette. Two additional lines, *8-1trunc* and *8-*

1HAtrunc, express truncated CLAG3 reporters with a stop codon introduced after the inserted cassette (Fig 1A, bottom and S1A Fig). We initially reasoned that these truncation constructs would yield a more flexible extracellular HiBiT epitope and provide insights into roles served by the downstream CLAG3 sequence. Although CLAG3 is a critical determinant of PSAC activity, CLAG3 knockout parasites are viable [26], possibly because other CLAG paralogs in *P. falciparum* compensate for CLAG3 loss. Thus, we expected that our modifications would be tolerated unless they produce a dominant-negative effect on nutrient uptake [27].

Immunoblotting with each cloned transfectant confirmed expression and revealed single bands of expected size. Probing with anti-CLAG3 confirmed loss of this antibody's C-terminal epitope in the *8-1trunc* clone and unchanged electrophoretic migration in *8-1* (Fig 1B, top). Both engineered CLAG3 isoforms were identified using a LgBiT probe that binds to HiBiT-tagged proteins to produce a luminescence signal (Fig 1B, bottom); the KC5 parent was not recognized by LgBiT, confirming specificity of this probe for the HiBiT tag. Similar results were obtained in the HA tandem-tagged parasites (Fig 1C), establishing faithful expression.

IFA confirmed and extended these findings. At the schizont stage, we detected each variant shortly after stage-specific synthesis under the genomic *clag3h* promoter (Fig 1D, upper group of images). While *8-1 HA* parasites trafficked the modified CLAG3 protein normally to developing rhoptries, the truncated tagged protein in *8-1HAtrunc* produced a more diffuse pattern with a small fraction reaching the rhoptry to colocalize with RhopH3, an associated protein that also contributes to PSAC formation [28].

At merozoite egress and reinvasion, rhoptry proteins are secreted into the next erythrocyte and deposited into the parasitophorous vacuole [29]. From there, through an incompletely understood interaction with the PTEX translocon, CLAG3 is exported into host cytosol for

trafficking to the host membrane [28,30]. Imaging revealed that the tandem-tagged CLAG3 protein in *8-1HA* trafficked as expected and colocalized with RhopH3 at the host cell surface (Fig 1D, lower group); an antibody specific for the CLAG3 c-terminus further confirmed this localization (S1B Fig). In contrast, the truncated CLAG3 in *8-1HAtrunc* parasites was less abundant, suggesting that its poor trafficking to rhoptries compromised delivery to the next erythrocyte upon reinvasion. The small pool of this protein delivered into trophozoites failed to be exported and did not colocalize with RhopH3 (Fig 1D, bottom row).

Stage-specific immunoblotting using *8-1HA* parasites revealed increases in CLAG3 abundance upon parasite maturation to the schizont stage (Fig 1E), consistent with synthesis of this and other RhopH proteins predominantly in the late-stage parasites [31]. Ring and trophozoite parasites contained lower amounts that reflect incomplete transfer from prior cycle schizonts during egress and reinvasion [28]. The truncated protein in *8-1HAtrunc* was detected in schizonts but not in ring- and trophozoite-stage parasites, further implicating a role of the CLAG3 c-terminal region in efficient transfer to rhoptries and new erythrocytes during invasion.

We next used co-immunoprecipitation on anti-HA beads to examine protein-protein interactions for these CLAG3 reporter proteins (Fig 1F, silver-stained gel). CLAG3 was recovered from *8-1HA* and *8-1HAtrunc* lysates but not from negative control *8-1* and *8-1trunc* lines (bands labeled "1"), confirming specific pull-down. RhopH2 and RhopH3, unrelated proteins that interact with CLAG3 [24], were recovered from *8-1HA* ("2" and "3"), albeit with lower efficiency than in experiments using CLAG3-tv2, an engineered control parasite that a full-length CLAG3 with a C-terminal HA epitope tag (Fig 1A, ref # [30]). This reduced yield may result from compromised binding and recovery with an internal HA epitope tag when compared to the C-terminal tag in CLAG3-tv2. Co-immunoprecipitation using *8-1HAtrunc*

yielded an unchanged RhopH2 band and a smaller band as expected for truncated CLAG3, but RhopH3 was not detected in these silver-stained gels (Fig 1F). Immunoblotting confirmed recovery of RhopH3 in *8-1HA* pull-downs and failed interaction with RhopH3 upon CLAG3 truncation (Fig 1G). The recent cryo-EM RhopH complex structure reveals that CLAG3 interacts with RhopH3 via two primary domains termed the CLAG3 "300 region" and "1300 loop" [30]. Because the 1300 loop is distal to the site of CLAG3 truncation in *8-1HAtrunc*, these findings suggest that this loop is required for stable CLAG3-RhopH3 interaction.

Kinetics of membrane insertion and surface exposure

We next monitored stage-specific CLAG3 surface exposure on infected erythrocytes with the RISE method. We measured luminescence resulting from complementation of the HiBiT tag by extracellular LgBiT (Fig 2A). Bioluminescence microscopy revealed an undetectable reporter signal on immature ring-infected erythrocytes (Fig 2B, left panels) on KC5 and both HiBiT tagged lines, consistent with the appearance of PSAC activity on infected cells only after parasite maturation [32]. In contrast, trophozoite-infected cells exhibited a surface-distributed luciferase signal specific to *8-1* (Fig 2B-C). The *8-1trunc* parasite matured normally but failed to produce a surface signal.

We then miniaturized this reporter assay into 96-well microplate wells and tracked CLAG3 exposure kinetics in cultures initiated shortly after invasion. Although both clones exhibited negligible signals for the first 16 h of the parasite cycle, this lag was followed by a rapid increase in CLAG3 membrane insertion to produce luminescence on *8-1* (Fig 2D, red circles). This signal reached a plateau between 30 and 44 h on *8-1*, during which *8-1trunc* parasites continued to produce minimal luminescence. At the end of the erythrocyte cycle (44-48 h), both transfectant cultures exhibited abruptly increased signals, consistent with merozoite egress and CLAG3

157 discharge into extracellular medium [31]. At the signal plateau, approximately 1/3 of the
158 CLAG3 within *8-1* infected cells had become surface-exposed based on measured reporter signal
159 before and after detergent release (Fig 2E, 36 h timepoint).

160 Prior studies of the CLAG3 HVR implicated exposure at the host cell surface based on this
161 motif's susceptibility to extracellular protease [9,25]. We therefore examined whether the
162 exposed HiBiT is also susceptible to external protease by measuring luminescence signals after a
163 brief protease treatment of trophozoite infected cells. While the background signal in KC5
164 parasites and the low-level signal from *8-1trunc* cells were not significantly affected by
165 extracellular protease treatment ($P > 0.1$, $n = 5$ independent trials each; Fig 2F), the large signal
166 produced by *8-1* infected cells was reduced by 39 ± 3% upon treatment with extracellular
167 protease ($P = 0.005$, $n = 5$), further confirming that our split NanoLuc assay faithfully reports on
168 CLAG3 exposure at the host cell surface.

169

170 **Failed export compromises channel-mediated permeability**

171 We next examined the effects of these CLAG3 modifications on nutrient uptake at the host
172 membrane. We tracked uptake of sorbitol, a sugar alcohol with high PSAC permeability, and
173 found that both the *8-1* and *8-1trunc* parasites increase host cell permeability (Fig 3A), as
174 expected from its requirement for intracellular pathogen survival [27,28]. Both *8-1* and *8-1trunc*
175 parasites exhibited lower sorbitol permeabilities than the parental KC5 (Fig 3B, $P < 10^{-4}$, $n = 20$-
176 21 trials each, one-way ANOVA with post-hoc tests), but uptake was preserved to a greater
177 extent in *8-1*. The reduced permeability in *8-1trunc* matched that of a recently reported CLAG3
178 knockout, *C3h-KO* ($P = 0.55$; ref # [26]), indicating that the truncated CLAG3 in this parasite

179 does not measurably contribute to PSAC activity. Failure to traffic and insert this protein in the
180 host membrane conservatively accounts for this phenotype (Fig 2).

181 CLAG3 cleavage within the HVR by extracellular protease compromises solute transport
182 [25]. Here, we found that pronase E treatment reduced channel-mediated transport in KC5 and
183 *8-1*, but had no effect in *8-1trunc* parasites (red traces, Fig 3A; Fig 3C, $P < 10^{-4}$, n = 10-11 trials,
184 one way ANOVA with post-hoc tests), also consistent with intracellular retention of the
185 truncated CLAG3 protein.

186 Immunoblots using an antibody directed against the CLAG3 C-terminus revealed single ~ 37
187 kDa cleavage products in KC5 and *8-1* (Fig 3D), corresponding to proteolysis at the surface-
188 exposed HVR and release of the distal fragment. Cleaved band intensities revealed that these
189 two parasites exported and inserted CLAG3 protein at the host membrane with indistinguishable
190 efficacies (Fig 3D, bar graph). Because *8-1trunc* parasites express a truncated CLAG3 not
191 recognized by this antibody, we then probed these blots with LgBiT. This approach is based on
192 visualization of HiBiT-tagged proteins via the luminescence generated upon LgBiT
193 complementation. This treatment reduced the band intensity in protein from *8-1* parasites but had
194 negligible effect on *8-1trunc* CLAG3 (Fig 3E, bar graph), consistent with proteolytic
195 degradation of an exposed HiBit tag only on *8-1* parasites.

196 These studies establish that CLAG3 must insert at the host membrane to contribute to PSAC
197 activity because the truncated protein in *8-1trunc* parasites has transport activity matching that of
198 a CLAG3-null parasite. They also reveal that proteolysis at a surface-exposed loop on CLAG3
199 compromises transport regardless of sequence as this site retained its susceptibility when
200 replaced by a HiBiT reporter.
201

Membrane insertion not compromised by increased extracellular loop size

To examine possible constraints on insertion of the CLAG3 HVR at the host membrane, we generated an additional transfectant carrying a larger 3xHA epitope tag after the HiBiT cassette (S1C Fig). Biochemical studies with *8-1HA* and this new parasite, *8-1-3HA*, revealed marked increases in luminescence signals as the extracellular loop size increased by 9 and 27 residues, respectively. Using matched numbers of trophozoite-stage parasites, we found a 7- and 50-fold higher luminescence signals from the *8-1HA* and *8-1-3HA* parasites (Fig 4A, red bars) than from *8-1*. The increases in luminescence were more modest when measured after cell lysis with detergent (black bars). Greater accentuation with intact cells than after lysis is consistent with steric hindrance or constrained HiBiT presentation in a minimal extracellular loop, as proposed for CLAG3 [25]. Addition of these tags also significantly increased susceptibility of the HiBiT reporter to extracellular protease, with the larger 3xHA tag producing a greater reduction in luminescence upon protease treatment (Fig 4B). Membrane insertion and surface exposure were further confirmed with immunoblotting (Fig 4C) and luminescence imaging, which revealed dramatically increased signals from intact cells (Fig 4D). These findings suggest improved LgBiT binding and reporter complementation upon adjacent HA epitope tagging, presumably because the size and negative charge of this tag improves accessibility at the extracellular loop and within soluble RhopH complexes upon detergent release.

These larger insertions into CLAG3 had modest effects on channel-mediated sorbitol uptake at the host membrane (Fig 4E). The resulting channels also retained quantitatively similar protease susceptibilities (Fig 4F), consistent with minimally affected CLAG3 insertion and PSAC formation at the host membrane.

Larger epitopes reveal complex regulation of CLAG3 membrane insertion

To further explore size and charge constraints on pathogen epitope presentation, we made additional transfectants containing multiple HiBiT tags with two different linker sizes (Fig 5A). As these constructs retained upstream and distal CLAG3 sequences, each modified protein trafficked normally through schizonts and was delivered into maturing trophozoite-infected cells (S2A-B Fig), where the increased size of the targeted protein was apparent in immunoblots (Fig 5B). Although immunofluorescence, sorbitol permeability measurements and protease susceptibility studies all suggested that CLAG3 failed to export and undergo host membrane insertion to enable PSAC activity in these lines (S2B Fig and Fig 5C), bioluminescence intensity analyses using RISE identified individual cells that presented CLAG3 on host cells (Fig 5D). Notably, while most cells in each of the largest multiple HiBiT constructs produced background signals, a few cells produced very bright signals that exceeded those seen on *8-1* parasites. These intense signals may reflect either reduced steric hindrance with larger, more flexible extracellular loops or signal amplification from HiBiT multiplicity on each protein. The markedly differing signals from individual cells is unexpected for these clonal lines. This observation suggests epigenetic control of CLAG3 export and host membrane insertion.

We tabulated the HVR sequences from 38 available CLAG3 sequences and compared their properties to those of the lines we have engineered. Although they are variant, the native HVR sequences tended to have a modest net negative charge (Fig 5E, black symbols). In contrast, the constructs containing more than one HiBit epitope were increasingly basic, yielding net positive charges on the at the extracellular loop (red symbols). Notably, the sequence in *8-1-3HA*, whose CLAG3 successfully inserted at the host membrane to produce remarkably bright luminescence using our RISE assays, had a higher molecular weight than that of *8-2*, which failed to traffic CLAG3 protein faithfully in most cells. It appears that the domain's net positive charge in *8-2*

and other multiple HiBit lines prevents trafficking and host membrane insertion. Along with structural constraints that ensure CLAG3-mediated nutrient uptake and evolutionary pressures to evade host immunity, the extracellular loop of this conserved protein family must also meet charge and size requirements for faithful trafficking and host membrane insertion.

Discussion

We present a new reporter that detects insertion of pathogen virulence antigens on their host cells. Our use of a split NanoLuc reporter is broadly applicable to a range of intracellular pathogens and will permit non-destructive kinetic tracking of antigens at the host cell surface. Some proteins targeted to underlying membranes, such as the parasitophorous vacuolar membrane of *Plasmodia*, *Toxoplasma*, and other parasites, may also be studied using selective permeabilization of the host membrane [33].

This reporter assay represents an important step toward understanding how pathogens interact with their host cells and will provide quantitative insights into the presentation of targeted antigens to the host immune system. We used this new technology to examine presentation of the conserved CLAG3 antigen on the surface of human erythrocytes. Associated nutrient channel transport, protein chemistry, and bioluminescence confocal microscopy studies all validated our new method.

Our findings implicate a revised model of CLAG3 trafficking. CLAG3 produced in schizonts remains inaccessible to extracellular LgBiT upon transfer to ring-infected cells; as the intracellular parasite matures, the protein is exported and inserts in the host membrane with kinetics that parallel the gradual appearance of the associated nutrient channel activity on trophozoite-infected cells. A C-terminal truncation that does not alter the reporter or its

upstream sequence compromised trafficking, abolished host membrane insertion, and reduced host cell permeability to levels seen in a recently reported CLAG3-null parasite. Using varied reporter insertions, we also uncovered complexities in this protein's insertion into the erythrocyte membrane; our studies suggest that both size and charge of the extracellular peptide loop determine host membrane insertion.

Our luminescence imaging studies revealed marked variation between cells in cloned multiple HiBit reporter lines, with some cells exhibiting high levels of CLAG3 exposure despite insertion of large reporter domains. This finding implicates an epigenetic, post-translational mechanism for regulating surface exposure. We propose that this may reflect altered expression of one or more parasite chaperone proteins in host cytosol [34] or post-translational modifications of CLAG3 [35,36]. Epigenetic control of antigen presentation on infected cells has, to our knowledge, not been proposed for any intracellular pathogens. This finding reveals the remarkable sophistication of malaria parasites in controlling their interactions with host plasma and further promotes immune evasion.

We envision that the quantitative and sensitive readout enabled by a small HiBiT epitope inserted at exposed antigen sites will unveil how pathogens modify their host cells while evading immune attack.

Materials and Methods

Parasite cultivation and transfection

The *P. falciparum* KC5 parasite clone and its engineered derivatives were cultivated in O+ human erythrocytes (Interstate Blood Bank, Inc.) at 5% hematocrit in standard RPMI 1640-based media (KD medical) supplemented with supplemented with 25 mM HEPES, 50 μg/mL

hypoxanthine, 0.5% NZ Microbiological BSA (MP Biomedicals), gentamicin and 28.6 mM $NaHCO_3$ (Gibco) at 37 °C under 90% N_2, 5% CO_2, 5% O_2.

CRISPR-Cas9 DNA transfection of parasites to produce reporter lines was performed using electroporation of pUF1-Cas9 and modified pL6 plasmids into uninfected erythrocytes as described previously [28]. Plasmids were constructed using synthetic double-stranded DNA (Integrated DNA Technologies) and In-Fusion cloning (Takara) into the pL6 plasmid. Single guide RNAs (sgRNA), selected using on-, off- and paralog specificity scores [37], were also introduced using In-Fusion. After erythrocyte electroporation and addition of schizont-staged parasites, the culture was selected with 1.5 μM DSM1 and 2.5 nM WR99210. After parasite outgrowth and PCR confirmation of integration, limiting dilution cloning was performed for all transfectant lines. All experiments were performed with sequence-verified clones.

Immunoblotting

Synchronous parasite cultures were harvested, percoll-enriched where indicated, and used for immunoblotting experiments after hypotonic lysis (7.5 mM Na_2HPO_4, 1 mM EDTA, 1 mM PMSF, pH 7.5) and solubilization in Laemmli sample buffer containing 6% SDS. When required, samples were matched with turbidity measurements at 700 nm. Proteins were separated by SDS-PAGE (4–15% Mini-PROTEAN TGX gel, Bio-RAD) and transferred to nitrocellulose membranes. After blocking with 3% skim milk powder in 150 mM NaCl, 20 mM TrisHCl, pH 7.4 with 0.1% Tween20 at RT for 1 h, primary antibodies were applied in the same blocking buffer at a 1:1000-1:3000 dilution and incubated overnight at 4 ˚C with gentle rocking. After three washes in 150 mM NaCl, 20 mM TrisHCl, pH 7.4 with 0.1% Tween20, HRP-conjugated secondary antibodies were added at 1:3000 dilution. The blot was incubated for 1 h

and washed three times. Imaging was performed after addition of Clarity Western ECL substrate (Bio-Rad) using the AI 680 imager (GE healthcare) or standard x-ray film exposure.

Where used, protease treatment was performed after washing and resuspending enriched trophozoite-infected cells in PBS-2 (150 mM NaCl, 20 mM Na_2HPO_4, 0.6 mM $CaCl_2$, 1 mM $MgCl_2$, pH 7.4) at 5% hematocrit with 1 mg/mL pronase E (Sigma) for 45-60 min at 37 ^oC. The treated cells and matched untreated cells were washed in PBS-2 with 1 mM PMSF at 4 ^oC before an additional wash in this buffer with 1 mM EDTA. After hypotonic lysis, the membrane fraction was harvested by ultracentrifugation (100,000 ×*g*, 1 h at 4 ˚C) and solubilized in Laemmli sample buffer as above.

Blots probed with LgBiT used the HiBiT blotting system kit (Promega). After protein transfer, nitrocellulose membranes were washed in 150 mM NaCl, 20 mM TrisHCl, pH 7.4 with 0.1% Tween20. LgBiT was applied in this blotting buffer at 1:200 dilution and incubated overnight at 4 ˚C with gentle rocking. Furimazine was then added in blotting buffer at a 1:500 dilution before imaging as above.

Band intensities were quantified using Image J software. Statistical analyses were based on three independent trials.

Coimmunoprecipitation

Schizont-stage infected cells were percoll-sorbitol enriched and lysed with 20 volumes of 10 mM Tris pH 7.5, 300 mM NaCl, 1% Triton-X100, 1 mM PMSF. After a 30 min incubation at 4 °C, solubilized proteins were separated by centrifugation (14,000 x *g*, 15 min, 4°C) and incubated with anti-HA affinity agarose beads (Sigma) with gentle mixing overnight at 4°C. After five washes, bound protein was eluted by addition of 2.5 mg/mL HA peptide in 10 mM Tris pH 7.5,

250 mM NaCl, 0.1% Triton-X100 for 30 min. Eluted proteins were resuspended in Laemmli sample buffer and subjected to SDS-PAGE.

Immunofluorescence assays

Indirect immunofluorescence assays were performed using air-dried thin smears after fixation with 1:1 acetone:methanol at -20 ˚C for 2 min. Slides were then dried, blocked with 3% milk in PBS for 1 h at RT, and incubated with primary antibodies in blocking buffer (mouse anti-CLAG3, 1:100; rabbit anti-RhopH3, 1:500; mouse anti-HA, 1:100) for 1.5 h at RT under coverslips. After two washes with chilled PBS, Alexa Fluor 488 or 594-conjugated secondary antibody at a 1:500 dilution and 10 µg/mL DAPI were added in blocking buffer and incubated for 30 min at RT. After washes and drying, slides were mounted with Prolong Diamond anti-fade mountant (Molecular Probes). Images were collected on a Leica SP8 microscope using a 64x oil immersion objective with serial 405 nm, 488 nm, or 594 nm excitation. Images were processed using Leica LAS X and Huygens software.

Enrichment of ring-infected cells

Ring-stage cultures were further synchronized by a 20 min incubation in 4% xylitol, a sugar alcohol with high PSAC permeability [38], to lyse mature infected cells. The culture was then resuspended and incubated in culture medium supplemented with 207 mM xylitol for 1 h at 37 ^{o}C. This cell suspension was then layered on a discontinuous percoll-xylitol gradient a bottom layer of 72% Percoll and an upper layer of 40% Percoll; both solutions were prepared in RPMI 1640 medium with 208 mM xylitol, 12.4 mM HEPES, and 16.3 mg/L BSA. After centrifugation

363 (10,000 x *g* for 30 min at 21 ºC), ring-stage infected cells at 65-90% parasitemia were harvested
364 and washed by dropwise addition of culture medium.
365
366 **Luminescence measurements and export kinetics**
367 Luminescence measurements were performed using percoll-enriched infected erythrocytes in
368 384 well microplates using the Nano-Glo HiBiT extracellular detection system (Promega). Cells
369 were resuspended at 0.2% hematocrit in culture medium diluted with two volumes of 200:1:50
370 buffer:LgBiT:Furimazine, according to the manufacture's protocol. After a 30 min RT
371 incubation, luminescence was measured using the Centro XS3 LB 960 reader (Berthold) or
372 Synergy Neo2 (BioTek) with a counting time of 0.5 s/well.
373 CLAG3 export kinetics were tracked using luminescence after seeding enriched ring-infected
374 cells in culture medium at 0.5% hematocrit into triplicate wells at 60 µL/well. The plates were
375 sealed with Breathe-Easy sealing membrane (RPI) and incubated at 37 ºC under 5% CO_2 in air.
376 At timed intervals, 40 µL of medium from selected wells was replaced with Nano-Glo HiBiT
377 extracellular buffer with LgBiT and furimazine substrate (Promega). Readings were taken after
378 a 30 min room temperature incubation as described above.
379
380 **Bioluminescence microscopy**
381 Erythrocytes infected with reporter parasite clones were imaged using a LV200 inverted
382 bioluminescence microscope with a temperature-controlled stage (Olympus). Enriched ring- or
383 trophozoite-infected erythrocytes were resuspended in culture medium at 2.5% hematocrit before
384 diluting 50x into Nano-Glo HiBiT extracellular buffer (Promega) with LgBiT and furimazine at
385 100x and 50x dilutions, respectively for a total volume of 100 µL in a 35 mm poly-D-lysine

386 coated coverslip dish (MatTek). Cells were allowed to settle at 37 °C for 25 min in the LV200
387 microscope before selecting fields of view for imaging. Bioluminescence images were collected
388 with a 45 min exposure under a 64x oil immersion objective. Images were visualized and
389 adjusted to 14 bit in LCmicro_2.2 software (Olympus).

390 Single cell luminescence intensities were quantified using a locally-developed macro that
391 uses the corresponding brightfield image to define the cell boundary. This macro reports
392 luminescence intensities over the cell, tabulating mean, max and min values along with the cell
393 2D area and is available upon request.

394

395 **Osmotic lysis assays**

396 The kinetics of PSAC-mediated sorbitol uptake and infected cell osmotic lysis were continuously
397 tracked as described previously [26]. Enriched trophozoite-stage infected cells were washed and
398 resuspended in 150 mM NaCl, 20 mM Na-HEPES buffer, 0.1 mg/mL BSA, pH 7.4. Solute
399 uptake was initiated by the addition of 280 mM sorbitol, 20 mM Na-HEPES, 0.1 mg/mL BSA,
400 pH 7.4. Concomitant uptake of sorbitol and water produces osmotic lysis at rates directly
401 proportional to PSAC sorbitol permeability. Lysis kinetics were continuously monitored using
402 transmittance of 700 nm light through the cell suspension. Osmotic lysis half-times, normalized
403 permeability estimates, and measures of protease effect were determined from the recordings
404 with locally developed code.

405

406 **Computational and statistical analyses**

407 CLAG3 sequences were downloaded from www.plasmodb.org and aligned using Multiple
408 Sequence Alignment (MUSCLE) to identify HVR sequences from available *P. falciparum*

409 paralogs. The molecular weight and net charge at pH 7.4 was calculated at
410 http://protcalc.sourceforge.net/.

411 Numerical data are shown as mean ± S.E.M. Data were analyzed in SigmaPlot 10.0 (Systat)
412 or Prizm 8 (GraphPad). Statistical significance was determined using unpaired or paired
413 Student's *t*-test or one-way ANOVA with *post hoc* Tukey's multiple comparisons test as
414 appropriate. Significance was accepted at $P < 0.05\%$.

415

416

417

418

419 ## Acknowledgements

420 We thank Gagan Saggu for help with immunofluorescence assays and David Jacobus for
421 WR99210. DSM1 (MRA-1161) was obtained through MR4 as part of the BEI Resources
422 Repository, NIAID, NIH.

423

Author contributions

Conceptualization: Jinfeng Shao, Sanjay A. Desai.

Data curation: Jinfeng Shao, Gunjan Arora, Javier Manzella-Lapeira, Joseph A. Brzostowski, Sanjay A. Desai.

Formal analysis: Jinfeng Shao, Gunjan Arora, Javier Manzella-Lapeira, Joseph A. Brzostowski, Sanjay A. Desai.

Investigation: Jinfeng Shao, Gunjan Arora, Javier Manzella-Lapeira.

Supervision: Sanjay A. Desai.

Writing – original draft: Jinfeng Shao, Sanjay A. Desai.

Writing – review & editing: Jinfeng Shao, Gunjan Arora, Javier Manzella-Lapeira, Joseph A. Brzostowski, Sanjay A. Desai.

Competing interests

The authors declare no competing interests.

References

1. Thakur A, Mikkelsen H, Jungersen G. Intracellular pathogens: host immunity and microbial persistence strategies. J Immunol Res. 2019; 2019:1356540. PMID: 31111075

2. Cornejo E, Schlaermann P, Mukherjee S. How to rewire the host cell: a home improvement guide for intracellular bacteria. J Cell Biol. 2017; 216: 3931-48. PMID: 29097627

3. Marti M, Baum J, Rug M, Tilley L, Cowman AF. Signal-mediated export of proteins from the malaria parasite to the host erythrocyte. J Cell Biol. 2005; 171: 587-92. PMID: 16301328

4. Laliberte J, Carruthers VB. Host cell manipulation by the human pathogen *Toxoplasma gondii*. Cell Mol Life Sci. 2008; 65: 1900-15. PMID: 18327664

5. Lee WC, Russell B, Renia L. Sticking for a cause: The falciparum malaria parasites cytoadherence paradigm. Front Immunol. 2019; 10:1444. PMID: 31316507

6. Yam XY, Preiser PR. Host immune evasion strategies of malaria blood stage parasite. Mol Biosyst. 2017; 13: 2498-508. PMID: 29091093

7. Desai SA. Why do malaria parasites increase host erythrocyte permeability? Trends Parasitol. 2014; 30: 151-9. PMID: 24507014

8. Mayhew TM, Lucocq JM. Developments in cell biology for quantitative immunoelectron microscopy based on thin sections: a review. Histochem Cell Biol. 2008; 130: 299-313. PMID: 18553098

9. Nguitragool W, Bokhari AA, Pillai AD, Rayavara K, Sharma P, Turpin B et al. Malaria parasite *clag3* genes determine channel-mediated nutrient uptake by infected red blood cells. Cell 2011; 145: 665-77. PMID: 21620134

10. Jouin H, Goguet de la Salmoniere YO, Behr C, Huyin Qan DM, Michel JC, Sarthou JL et al. Flow cytometry detection of surface antigens on fresh, unfixed red blood cells infected by *Plasmodium falciparum*. J Immunol Methods. 1995; 179: 1-12. PMID: 7868917

11. Florens L, Liu X, Wang Y, Yang S, Schwartz O, Peglar M et al. Proteomics approach reveals novel proteins on the surface of malaria-infected erythrocytes. Mol Biochem Parasitol. 2004; 135: 1-11. PMID: 15287581

12. Cohn JV, Alkhalil A, Wagner MA, Rajapandi T, Desai SA. Extracellular lysines on the plasmodial surface anion channel involved in Na^+ exclusion. Mol Biochem Parasitol. 2003; 132: 27-34. PMID: 14563534

13. Taraschi TF, Trelka D, Martinez S, Schneider T, O'Donnell ME. Vesicle-mediated trafficking of parasite proteins to the host cell cytosol and erythrocyte surface membrane in *Plasmodium falciparum* infected erythrocytes. Int J Parasitol. 2001; 31: 1381-91. PMID: 11566305

14. Papakrivos J, Newbold CI, Lingelbach K. A potential novel mechanism for the insertion of a membrane protein revealed by a biochemical analysis of the *Plasmodium falciparum* cytoadherence molecule PfEMP-1. Mol Microbiol. 2005; 55: 1272-84. PMID: 15686570

15. Wehrman TS, Casipit CL, Gewertz NM, Blau HM. Enzymatic detection of protein translocation. Nat Methods. 2005; 2: 521-7. PMID: 15973423

16. Joffre OP, Segura E, Savina A, Amigorena S. Cross-presentation by dendritic cells. Nat Rev Immunol. 2012; 12: 557-69. PMID: 22790179

17. Azevedo MF, Nie CQ, Elsworth B, Charnaud SC, Sanders PR, Crabb BS et al. *Plasmodium falciparum* transfected with ultra bright NanoLuc luciferase offers high sensitivity detection for the screening of growth and cellular trafficking inhibitors. PLoS One. 2014; 9: e112571. PMID: 25392998

18. Dixon AS, Schwinn MK, Hall MP, Zimmerman K, Otto P, Lubben TH et al. NanoLuc complementation reporter optimized for accurate measurement of protein interactions in cells. ACS Chem Biol. 2016; 11: 400-8. PMID: 26569370

19. Knuepfer E, Rug M, Klonis N, Tilley L, Cowman AF. Trafficking of the major virulence factor to the surface of transfected *P. falciparum*-infected erythrocytes. Blood. 2005; 105: 4078-87. PMID: 15692070

20. Llora-Batlle O, Tinto-Font E, Cortes A. Transcriptional variation in malaria parasites: why and how. Brief Funct Genomics. 2019; 18: 329-41. PMID: 31114839

21. Cortes A, Carret C, Kaneko O, Yim Lim BY, Ivens A, Holder AA. Epigenetic silencing of *Plasmodium falciparum* genes linked to erythrocyte invasion. PLoS Pathog. 2007; 3: e107. PMID:17676953

22. Iriko H, Kaneko O, Otsuki H, Tsuboi T, Su XZ, Tanabe K et al. Diversity and evolution of the *rhoph1*/*clag* multigene family of *Plasmodium falciparum*. Mol Biochem Parasitol. 2008; 158(1): 11-21. PMID: 18155305

23. Gupta A, Balabaskaran-Nina P, Nguitragool W, Saggu GS, Schureck MA, Desai SA. CLAG3 self-associates in malaria parasites and quantitatively determines nutrient uptake channels at the host membrane. mBio. 2018; 9: e02293-17. PMID: 29739907

24. Gupta A, Thiruvengadam G, Desai SA. The conserved *clag* multigene family of malaria parasites: essential roles in host-pathogen interaction. Drug Resist Updat. 2015; 18:47-54. PMID: 25467627

25. Nguitragool W, Rayavara K, Desai SA. Proteolysis at a specific extracellular residue implicates integral membrane CLAG3 in malaria parasite nutrient channels. PLoS One 2014; 9: e93759. PMID: 24699906

26. Gupta A, Bokhari AAB, Pillai AD, Crater AK, Gezelle J, Saggu G et al. Complex nutrient channel phenotypes despite Mendelian inheritance in a *Plasmodium falciparum* genetic cross. PLoS Pathog. 2020; 16: e1008363. PMID: 32069335

27. Pillai AD, Nguitragool W, Lyko B, Dolinta K, Butler MM, Nguyen ST et al. Solute restriction reveals an essential role for *clag3*-associated channels in malaria parasite nutrient acquisition. Mol Pharmacol. 2012; 82: 1104-14. PMID: 22949525

28. Ito D, Schureck MA, Desai SA. An essential dual-function complex mediates erythrocyte invasion and channel-mediated nutrient uptake in malaria parasites. Elife. 2017; 6:e23485. PMID: 28221136

29. Ben CR, Lentini G, Soldati-Favre D. Biogenesis and discharge of the rhoptries: Key organelles for entry and hijack of host cells by the Apicomplexa. Mol Microbiol. 2021; 115: 453-65. PMID: 33368727

30. Schureck MA, Darling JE, Merk A, Shao J, Daggupati G, Srinivasan P et al. Malaria parasites use a soluble RhopH complex for erythrocyte invasion and an integral form for nutrient uptake. Elife 2021; 10: e65282. PMID: 33393463

31. Ling IT, Florens L, Dluzewski AR, Kaneko O, Grainger M, Yim Lim BY et al. The *Plasmodium falciparum clag9* gene encodes a rhoptry protein that is transferred to the host erythrocyte upon invasion. Mol Microbiol. 2004; 52: 107-18. PMID: 15049814

32. Kutner S, Baruch D, Ginsburg H, Cabantchik ZI. Alterations in membrane permeability of malaria-infected human erythrocytes are related to the growth stage of the parasite. Biochim Biophys Acta. 1982; 687: 113-7. PMID: 0007041976

33. Jackson KE, Spielmann T, Hanssen E, Adisa A, Separovic F, Dixon MW et al. Selective permeabilization of the host cell membrane of *Plasmodium falciparum*-infected red blood cells with streptolysin O and equinatoxin II. Biochem J. 2007; 403: 167-75. PMID: 17155936

34. Zhang Q, Ma C, Oberli A, Zinz A, Engels S, Przyborski JM. Proteomic analysis of exported chaperone/co-chaperone complexes of *P. falciparum* reveals an array of complex protein-protein interactions. Sci Rep. 2017; 7:42188. PMID: 28218284

35. Cobbold SA, Santos JM, Ochoa A, Perlman DH, Llinas M. Proteome-wide analysis reveals widespread lysine acetylation of major protein complexes in the malaria parasite. Sci Rep. 2016; 6:19722. PMID: 26813983

36. Pease BN, Huttlin EL, Jedrychowski MP, Talevich E, Harmon J, Dillman T et al. Global analysis of protein expression and phosphorylation of three stages of *Plasmodium falciparum* intraerythrocytic development. J Proteome Res. 2013; 12: 4028-45. PMID: 23914800

542 37. Ribeiro JM, Garriga M, Potchen N, Crater AK, Gupta A, Ito D et al. Guide RNA selection
543 for CRISPR-Cas9 transfections in *Plasmodium falciparum*. Int J Parasitol. 2018; 48:825-
544 32. PMID: 29906414

545 38. Bokhari AA, Solomon T, Desai SA. Two distinct mechanisms of transport through the
546 plasmodial surface anion channel. J Membr Biol. 2008; 226: 27-34. PMID: 19050955

547

Figure Legends

Fig. 1. Design and production of host membrane-exposed split-reporter antigens. (A) Schematic shows native and modified CLAG3 topology at the host erythrocyte surface (left and right top images, respectively). The native HVR sequence is replaced by varied HiBiT reporter cassettes. Engineered lines are shown with ribbon diagrams at the bottom. **(B)** Immunoblots of matched total cell lysates from indicated lines, probed with antibody against a C-terminal CLAG3 epitope (top) or with LgBiT (bottom). *8-1trunc* is recognized by LgBiT but not by anti-CLAG3. **(C)** Immunoblots showing recognition of HA-tagged lines with anti-HA and LgBiT. **(D)** Indirect immunofluorescence assays (IFA) of indicated proteins in wild-type (WT) and transfected lines. In schizonts (top panels), CLAG3 colocalizes with RhopH3 in apical rhoptries (puncta) in *8-1HA*, but has a more diffuse distribution in *8-1HAtrunc.* IFA with trophozoite-stage parasites (bottom panels) reveals normal export of CLAG3 and colocalization with RhopH3 at the host membrane in *8-1HA* but a reduced signal with failed export in *8-1HAtrunc.* Scale bars, 5 mm. **(E)** Immunoblots showing stage-specific CLAG3 abundance in indicated lines (top row, probed with LgBiT). The truncated protein in *8-1HAtrunc* is detected in schizonts (S) but not rings or trophozoites (R and T). Bottom row, aldolase loading control. **(F)** Silver-stained gel showing co-immunoprecipitation using anti-HA beads and indicated parasite lysates. WT, *8-1*, and *8-1trunc* represent no-HA negative controls. Yellow 1, 2, and 3 labels indicate CLAG3, RhopH2, and RhopH3, respectively. **(G)** Immunoblots using eluates from panel **F**, probed with anti-RhopH3 and anti-HA for the CLAG3 bait protein.

Fig. 2. Faithful tracking of host membrane insertion. (A) Schematic showing parasite developmental stages and host membrane insertion-dependent luminescence. After invasion, the tagged CLAG3 protein is deposited into the parasitophorous vacuole before export and eventual

572 insertion at the host membrane. Interaction between extracellular LgBiT and the surface-
573 exposed HiBiT tag on *8-1* yields luminescence at mature parasite stages (purple glow). **(B)**
574 Bioluminescence microscopy images showing undetectable signals on immature ring-infected
575 cells (left panels), but a bright luminescence signal on *8-1* infected cells at the trophozoite stage
576 (right panels). KC5 and *8-1trunc* parasites yield negligible signals. Scale bars, 10 μm. **(C)**
577 "Zoom in" of a single *8-1* infected cell from panel **B**, showing surface distribution of
578 luminescence signal. Scale bar, 2 μm. **(D)** Luminescence kinetics over parasite development,
579 showing CLAG3 membrane insertion in *8-1* but not *8-1trunc* (red and black symbols,
580 respectively; mean ± S.E.M. of 3 replicate wells, representative of 3 independent trials).
581 Enriched synchronized early ring-infected cells seeded at $t = 0$. Increased signals at 48 h in both
582 parasites reflect parasite egress and release of intracellular reporter protein. **(E)** Mean ± S.E.M.
583 CLAG3 exposure on indicated lines at 36 h (*, $P = 0.03$, $n = 3$ trials), calculated as the
584 luminescence signal normalized to total signal after cell lysis. **(F)** Mean ± S.E.M. luminescence
585 signals from enriched trophozoite-infected cells without and with extracellular protease treatment
586 (black and red bars, respectively; *, $P = 0.005$, $n = 5$).
587
588 **Fig. 3. Modest effect of the reporter tag on CLAG3 export and on channel-mediated**
589 **nutrient uptake. (A)** Kinetics of osmotic lysis due to sorbitol uptake by indicated lines without
590 or with pretreatment with pronase E (black and red traces, respectively). **(B)** Apparent sorbitol
591 permeability coefficients from experiments as in panel A without protease treatment, calculated
592 as 1/halftime of osmotic lysis. *, $P < 10^{-4}$. **(C)** Pronase E-resistant transport activity for
593 indicated lines, normalized to 100% for matched untreated controls. *, $P < 10^{-4}$. **(D)** Anti-
594 CLAG3 immunoblot showing a 37 kDa C-terminal cleavage product released by pronase E

595 treatment. Bar graph shows quantified fractional band intensity of the cleavage product (mean ±
596 S.E.M. 2 independent trials). **(E)** Blot probed with LgBiT showing reduction in the 150 kDa
597 full length CLAG3 protein upon protease treatment. Bar graph, band intensities after protease
598 treatment, normalized to 100% without protease (2 independent trials).
599
600 **Fig. 4. Addition of HA and 3xHA tags improve reporter signal and does not compromise**
601 **host membrane insertion. (A)** Mean ± S.E.M. luminescence signals from indicated parasite
602 clones using matched amounts of enriched trophozoite-infected cells. Red and black bars
603 represent intact and lysed cells, respectively (*, $P = 10^{-4}$, one-way ANOVA, $n = 3$ independent
604 trials). Signals are shown after normalization of *8-1* readings to 1.0 in each trial. Immunoblot
605 shows representative loading control for matching protein contents from one of the three trials.
606 **(B)** Mean ± S.E.M. luminescence signals remaining after extracellular protease treatment of
607 intact cells from indicated lines, normalized to 100% for no protease effect (*, $P = 0.0002$, $n = 3$-
608 6 for each clone). **(C)** Anti-CLAG3 immunoblot showing C-terminal cleavage product released
609 by extracellular pronase E treatment. **(D)** Bioluminescence microscopy showing increased
610 signals from individual cells when 1HA and 3HA tags are added to the HiBit reporter. Scale
611 bars, 5 µm. **(E)** Mean ± S.E.M. sorbitol permeabilities for indicated parasites, determined from
612 osmotic lysis experiments ($n = 5$-21 trials each). **(F)** % of transport resistant to treatment with
613 extracellular pronase E ($n = 4$-11 trials). Channel-mediated transport is modestly affected in
614 these lines.
615
616 **Fig. 5. Large reporter inserts reveal complex regulation of CLAG3 insertion at the host**
617 **membrane. (A)** To-scale schematic showing multi-HiBiT inserts and sizes of linkers between

618 elements. The parasite names reflect the predominant linker size (in residues) followed by the
619 number of introduced HiBiTs. **(B)** Anti-CLAG3 immunoblot confirming the expected increase
620 in CLAG3 size with each construct. **(C)** PSAC activity in transfected clones. Top left, osmotic
621 lysis kinetics for the KC5 parent (black), *8-1* (red), *8-2* (blue), and *8-1trunc* (grey). Right, mean
622 ± S.E.M. apparent sorbitol permeability coefficients for indicated lines; red dotted line, mean for
623 the C*3h-KO* knockout line. Note that all multi-HiBiT inserts have permeabilities
624 indistinguishable from those of the CLAG3 knockout. Bottom left, *8-2* osmotic lysis kinetics
625 with and without protease treatment (red and black, respectively), showing that transport is not
626 protease sensitive in this line. Bottom right, mean ± S.E.M. % of transport resistant to
627 extracellular pronase E treatment. In contrast to the CLAG3 export competent KC5 and *8-1*
628 lines, transport linked to the multi-HiBiT inserts is resistant to extracellular pronase. **(D)**
629 Microscopy images showing rare luminescent cells in the *8-5* reporter line. Jitter plot shows
630 single cell intensities of indicated lines. Break points were selected based on the range of
631 intensities in the KC5 and *8-1* controls. Note that while most cells are negative in the multi-
632 HiBiT constructs, a small number have very high signals in each reporter line. **(E)** 2D plot
633 showing molecular weight (MW) and net charge at pH 7.4 for the CLAG3 HVR region from 38
634 available sequences (black circles) and the indicated engineered substitutions (red symbols).
635

636 ## Supporting Figure Legends

637 **S1 Fig. Construction and validation of reporter protein for host membrane insertion. (A)**
638 Sequences of the modified CLAG3 locus in *8-1* and *8-1HA* reporter lines aligned with the
639 parental KC5 CLAG3h and CLAG3.1 and CLAG3.2 from divergent *P. falciparum* lines (7G8
640 and Dd2 from Brazil and Indochina, respectively). The HVR sequences from wild-type lines is

641 highlighted in grey; introduced HiBiT is shown with magenta highlight. HA tag is underlined;
642 the sites where stop codons were introduced to produce *8-1trunc* and *8-1HAtrunc* are marked
643 with red arrows. Identical and conserved residues that flank the HVR are in red and blue,
644 respectively. Note the length polymorphism in native HVR sequences; the modification to
645 produce *8-1HA* increases the length of this extracellular motif. **(B)** IFA of trophozoite-stage
646 parasites probed with a CLAG3-specific antibody directed against a C-terminal epitope [9].
647 Scale bar, 5 μm. Notice unchanged export and colocalization with RhopH3 in *8-1* and *8-1HA*
648 parasites. **(C)** Modified CLAG3 locus sequence in the *8-1-3HA* parasite with color-coding as in
649 panel **A**. The 3xHA tag is underlined.
650
651 **S2 Fig. Trafficking and membrane insertion for large multi-HiBiT insertions into the**
652 **CLAG3 HVR.** IFA micrographs of indicated lines at the schizont and trophozoite stages (panels
653 **A** and **B**, respectively), showing that each construct is faithfully trafficked to rhoptry organelles
654 in schizonts, but that the multi-HiBiT lines do not export CLAG3 to the host membrane of most
655 trophozoite-infected cells. Scale bars, 5 μm. **(C)** Anti-CLAG3 immunoblot showing that
656 chymotrypsin releases a ~ 35 kDa cleavage product in KC5 and *8-1* parasites, but that cleavage
657 is not detected in studies with the indicated multi-HiBiT lines.

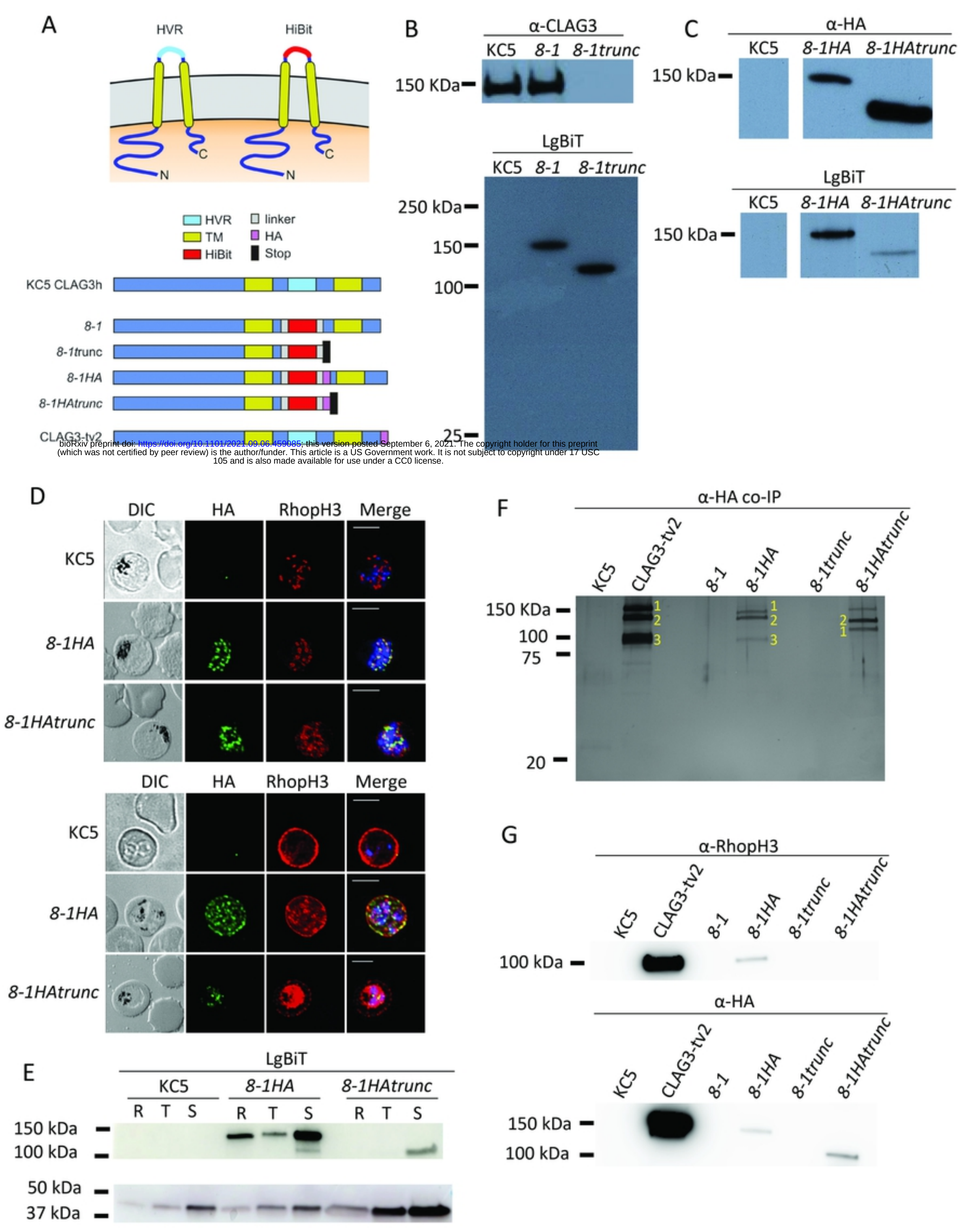

Figure 1

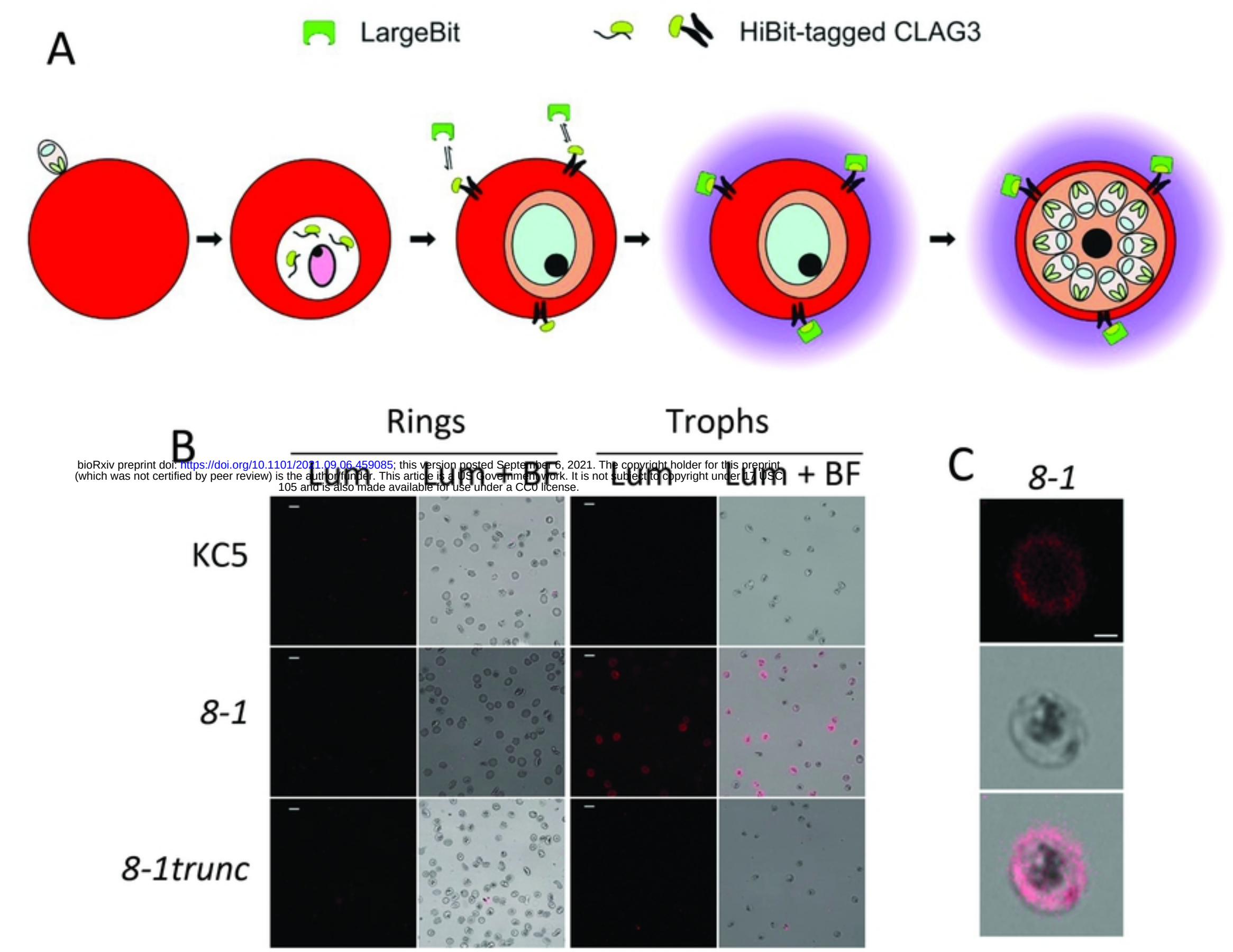

Figure 2

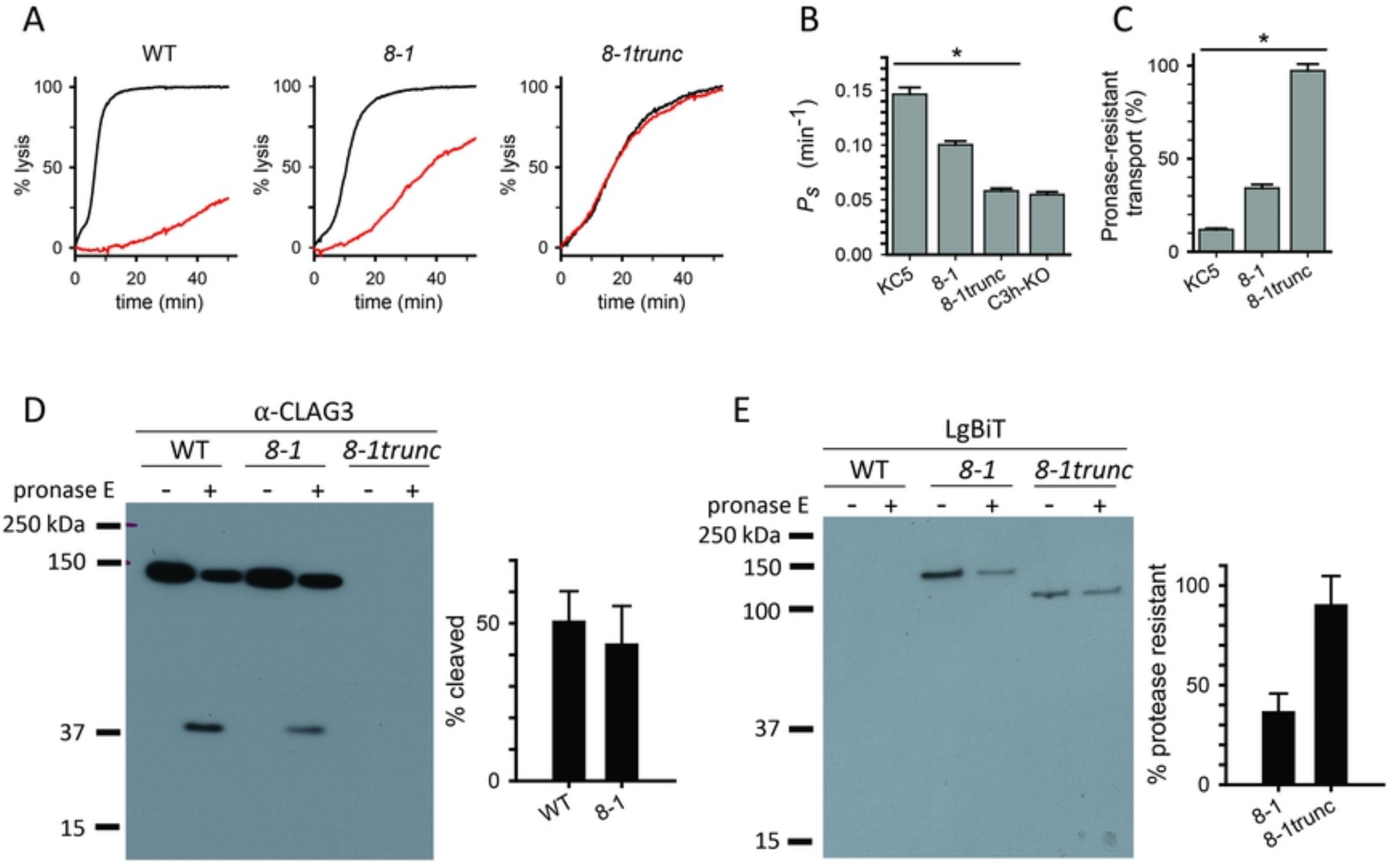
A
WT
8-1
8-1trunc
% lysis
time (min)
B
P_S (min^{-1})
KC5
8-1
8-1trunc
C3h-KO
C
Pronase-resistant transport (%)
KC5
8-1
8-1trunc
D
α-CLAG3
WT
8-1
8-1trunc
pronase E
250 kDa
150
37
15
% cleaved
E
LgBiT
WT
8-1
8-1trunc
pronase E
250 kDa
150
100
37
15
% protease resistant

Figure 3

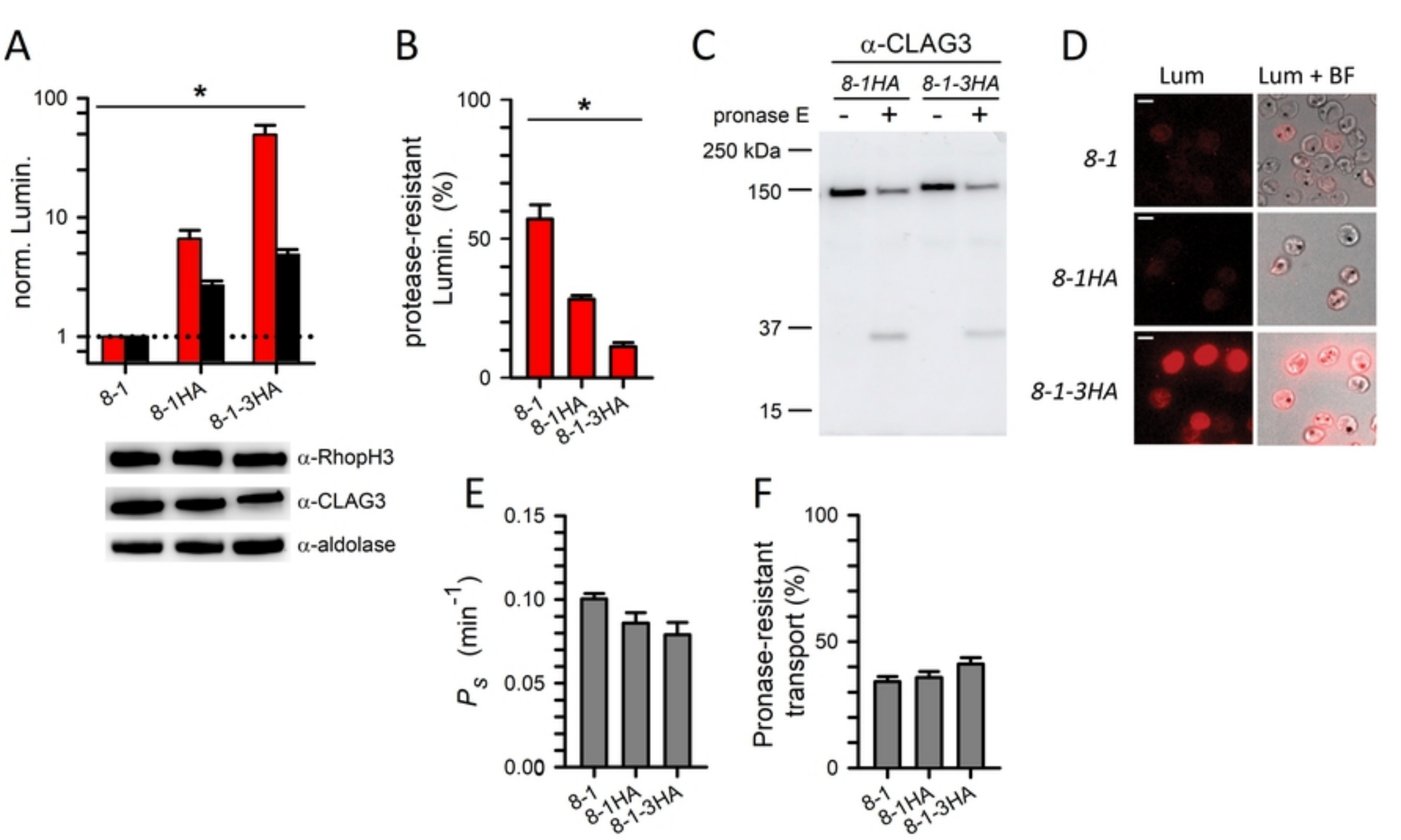
A
100
10
1
norm. Lumin.
*
8-1
8-1HA
8-1-3HA
α-RhopH3
α-CLAG3
α-aldolase
B
100
50
0
protease-resistant Lumin. (%)
*
8-1
8-1HA
8-1-3HA
C
α-CLAG3
8-1HA
8-1-3HA
pronase E
- + - +
250 kDa
150
37
15
D
Lum
Lum + BF
8-1
8-1HA
8-1-3HA
E
0.15
0.10
0.05
0.00
P_s (min^{-1})
8-1
8-1HA
8-1-3HA
F
100
50
0
Pronase-resistant transport (%)
8-1
8-1HA
8-1-3HA

Figure 4

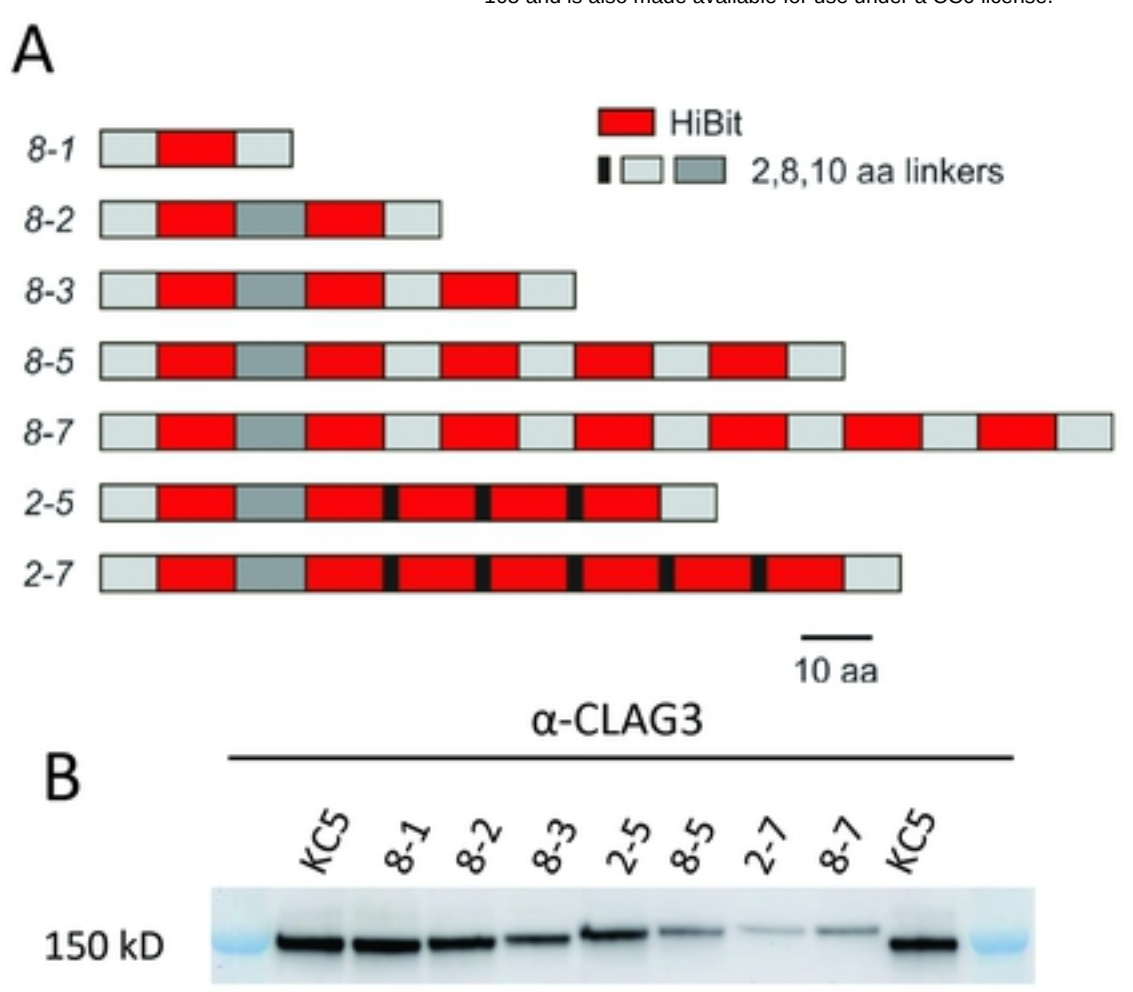

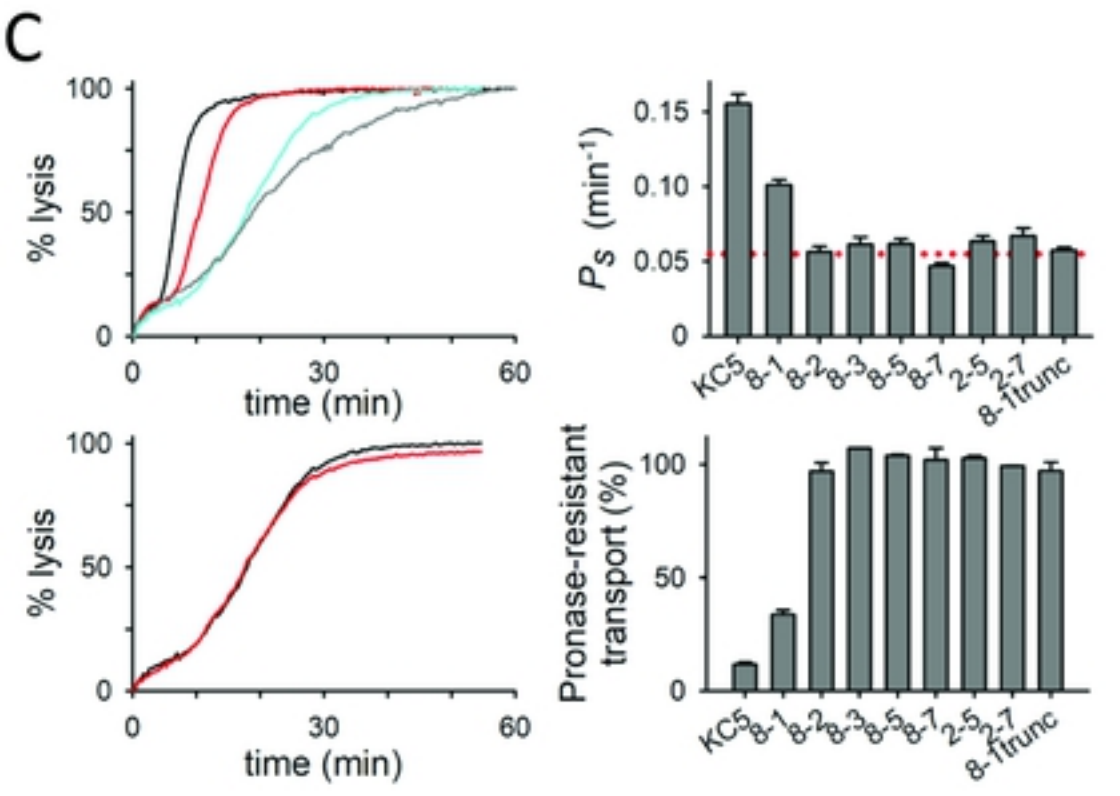

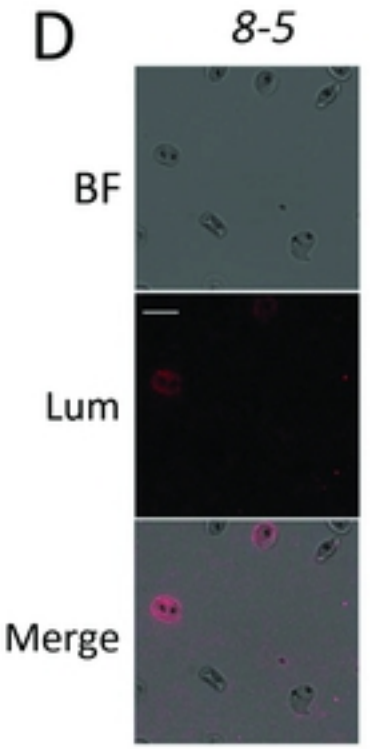

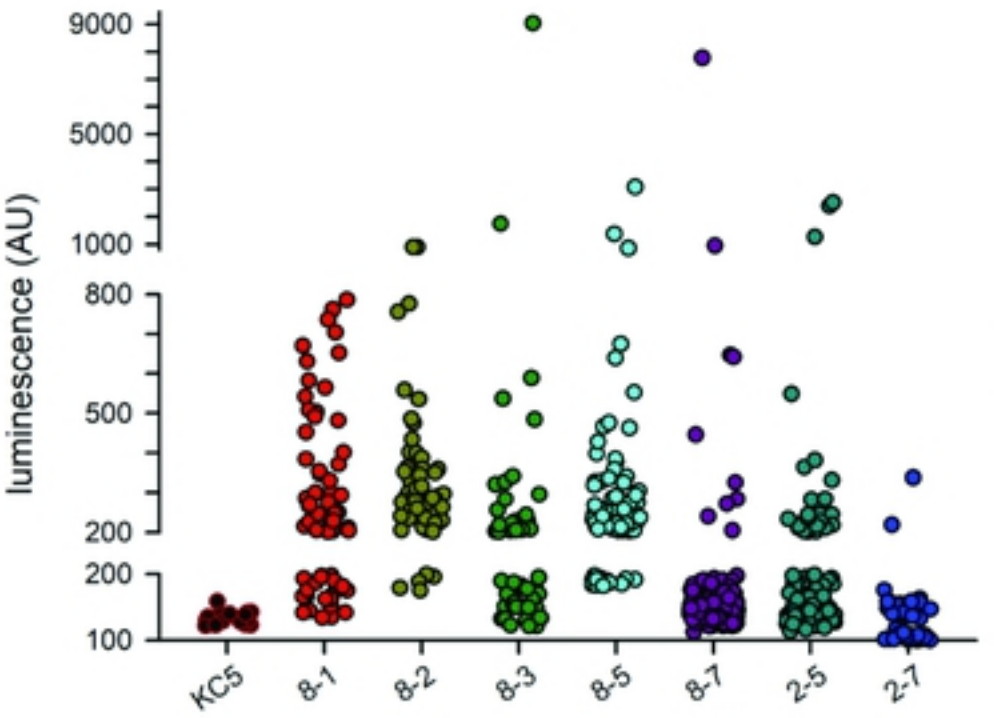

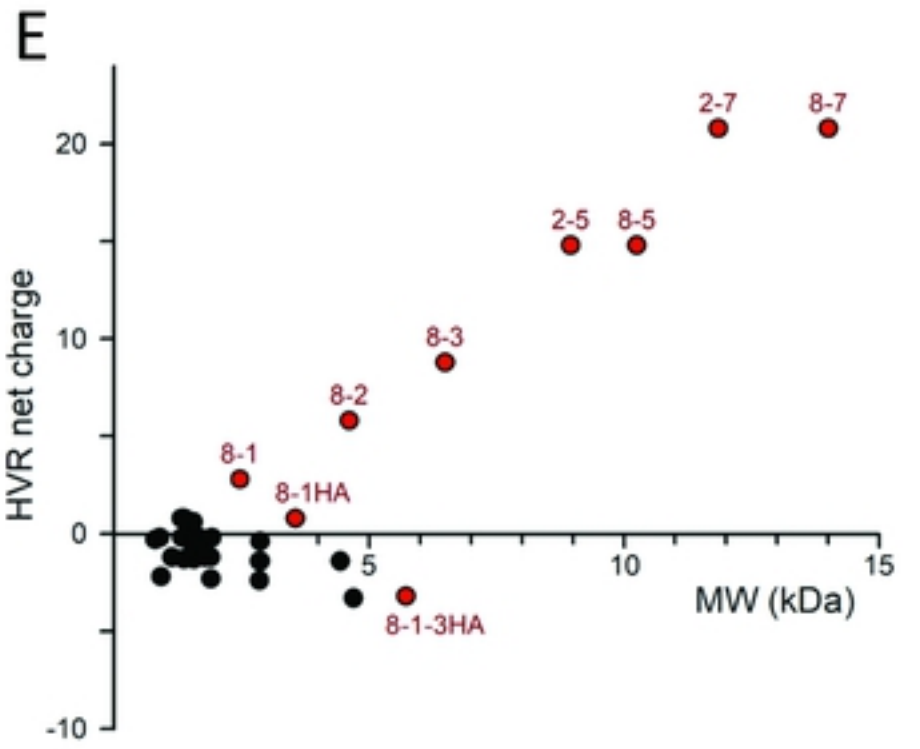

Figure 5